

Estimating the frame potential of large-scale quantum circuit sampling using tensor networks up to 50 qubits

Minzhao Liu,^{1,2,*} Junyu Liu^{*,3,4,5,6,†} Yuri Alexeev,^{2,4,‡} and Liang Jiang^{3,4,§}

¹*Department of Physics, The University of Chicago, Chicago, IL 60637, USA*

²*Computational Science Division, Argonne National Laboratory, Lemont, IL 60439, USA*

³*Pritzker School of Molecular Engineering, The University of Chicago, Chicago, IL 60637, USA*

⁴*Chicago Quantum Exchange, Chicago, IL 60637, USA*

⁵*Kadanoff Center for Theoretical Physics, The University of Chicago, Chicago, IL 60637, USA*

⁶*qBraid Co., Harper Court 5235, Chicago, IL 60615, USA*

(Dated: May 23, 2022)

We develop numerical protocols for estimating the frame potential, the 2-norm distance between a given ensemble and the exact Haar randomness, using the **QTensor** platform.

Our tensor-network-based algorithm has polynomial complexity for shallow circuits and is high performing using CPU and GPU parallelism. We apply the above methods to two problems: the Brown–Susskind conjecture, with local and parallel random circuits in terms of the Haar distance and the approximate k -design properties of the hardware efficient ansätze in quantum machine learning, which induce the barren plateau problem. We estimate frame potentials with these ensembles up to 50 qubits and $k = 5$, examine the Haar distance of the hardware-efficient ansätze, and verify the Brown–Susskind conjecture numerically. Our work shows that large-scale tensor network simulations could provide important hints toward open problems in quantum information science.

*: Corresponding author.

I. INTRODUCTION

Quantum computing might provide significant improvement of computational powers for current information technologies [1–3]. In the noisy intermediate-scale quantum (NISQ) era, an important question for near-term quantum computing is whether quantum devices are able to realize strong computational advantage against existing classical devices and resolve hard problems that no existing classical computers can resolve [4]. Recently, Google and the University of Science and Technology of China, in experiments involving boson sampling [5, 6], claim to have realized quantum advantage in their quantum devices, disproving the extended Church–Turing thesis. These experiments are considered milestones toward full-scale quantum computing. Another recent study suggests the possibility of achieving quantum advantage in runtime over specialized state-of-the-art heuristic algorithms to solve the Maximum Independent Set problem using Rydberg atom arrays [7].

Despite the great experimental success in quantum devices, however, the capability of classical computation is also rapidly developing. It is interesting and important to think about where the boundary of classical computation of the same process is and to understand the underlying physics of the quantum supremacy experiments through

classical simulation [5]. Tensor network methods are incredibly useful for simulating quantum circuits [8–10]. Originating from approximately solving ground states of quantum many-body systems, tensor network methods find approximate solutions when the bond dimension of contracted tensors and the required entanglement of the system are under control [8]. Tensor network methods are also widely used for investigating sampling experiments with random quantum architectures, which are helpful for verifying the quantum supremacy experiments [11–14].

In this work we develop novel tensor network methods and perform classical random circuit sampling experiments up to 50 qubits. Random circuit sampling experiments are important components of near-term characterizations of quantum advantage [15]. Ensembles of random circuits could provide implementable constructions of approximate unitary k -designs [16–18], quantum information scramblers [19], solvable many-body physics models [20], predictable variational ansätze for quantum machine learning [21–23], good quantum decouplers for quantum channel and quantum error correction codes [24, 25], and efficient representatives of quantum randomness. To measure how close a given random circuit ensemble is to uniform, Haar randomness over the unitary group, we develop algorithms to evaluate the frame potential, the 2-norm distance toward full Haar randomness [26–28]. The frame potential is a user-friendly measure of how random a given ensemble is in terms of operator norms: the smaller the frame potential is, the more chaotic and more complicated the ensembles are, and the more easily we can achieve computational advantages [29, 30]. In fact, in certain quantum cryptographic tools, concepts identical or similar to approximate k -designs are used, making use of the exponential separation of complexities between classical and quantum computations

* mliu6@uchicago.edu

† junyuliu@uchicago.edu

‡ yuri@anl.gov

§ liangjiang@uchicago.edu

[31–38]. The efficient tensor network contraction algorithm is developed in the **QTensor** framework [39–41].

In particular, we show the following applications of our computational tools. First, we evaluate the k -design time of the local and parallel random circuits through the frame potential. A long-term open problem is to prove the linear scrambling property of random circuits, where they approach approximate k -designs at depth $\mathcal{O}(nk)$ with n qudits [16–18, 29, 31, 42–47]. Although lower and upper bounds are given, there is no known proof of the k -design time for general local dimension q and $k \geq 3$ [18, 47]. According to [47], the linear increase of the k -design time will lead to a proof of the Brown–Susskind conjecture, a statement where random circuits have linear growth of the circuit complexity with insights from black hole physics [48, 49]. Recently, the complexity statement was proved in [50] for a different definition of circuit complexity compared with [47]. Thus, a validation of the k -design time measured in the frame potential will immediately lead to an alternative verification of the Brown–Susskind conjecture, with the complexity defined in [47]. Using our tools, we verify the linear scaling of the k -design time up to 50 qubits and $q = 2$. Our research also provides important data on the prefactors beyond the scaling through numerical simulations, which will be helpful to further the understanding of theoretical computer scientists.

Moreover, we use our tools to evaluate the frame potential of the randomized hardware-efficient variational ansatz used in [21]. *Barren plateau* is a term referring to the slowness of the variational angle updates during the gradient descent dynamics of quantum machine learning. When the variational ansätze for variational quantum simulation, variational quantum optimization, and quantum machine learning [51–63] are random enough, the gradient descent updates of variational angles will be suppressed by the dimension of Hilbert space, requiring exponential precision to implement quantum control of variational angles [23]. The quadratic fluctuations considered in [21] will be suppressed with an assumption of 2-design, which is claimed to be satisfied by their hardware-efficient variational ansätze. For higher moments, higher k -designs are required. A study of how far from a given variational assumption to a unitary k -design is important in order to understand how large the barren plateau is and how to mitigate them through designs of variational circuits. In our work we find that for several k s, the randomized hardware-efficient ansätze are efficient scramblers: the frame potential decays exponentially during an increase in circuit depth.

Our paper is organized as follows. In Section II we give an overview of the theory of frame potentials. In Section III we present a novel tensor network algorithm for evaluating frame potentials efficiently in high-performance computing. In Section IV we discuss our numerical results and implications. In Section V we summarize our work and provide some future research directions.

II. FRAME POTENTIAL

Given an ensemble \mathcal{E} of unitaries with a probability measure, we are interested in its randomness and therefore closeness to the unitary group. Truly random unitaries from the unitary group have the *Haar* measure. Such closeness is measured by how well the ensemble approximates the first k moments of the unitary group. To this end, a k -fold twirling channel

$$\Phi_{\mathcal{E}}^{(k)}(\mathcal{O}) = \int_{\mathcal{E}} dU U^{\otimes k}(\mathcal{O})U^{\dagger \otimes k} \quad (1)$$

is defined for the ensemble. If the unitary ensemble approximates the k th moment of the unitary group, the distance between the k -fold channel defined for the ensemble and the Haar unitaries (measured by the diamond norm) is bounded by ϵ :

$$\|\Phi_{\mathcal{E}}^{(k)} - \Phi_{\text{Haar}}^{(k)}\|_{\diamond} \leq \epsilon. \quad (2)$$

Such \mathcal{E} is said to be an ϵ -approximate k -design. The diamond norm of the channels is not numerically friendly, however. A quantity more suitable for numerical evaluation, which is also discussed in the context of k -designs, is the *frame potential* \mathcal{F} , given by [64]

$$\mathcal{F}_{\mathcal{E}}^{(k)} = \int_{U, V \in \mathcal{E}} dU dV |\text{Tr}(U^{\dagger}V)|^{2k}. \quad (3)$$

Specifically, it relates to the aforementioned definition of ϵ -approximate k -designs as follows [18]:

$$\|\Phi_{\mathcal{E}}^{(k)} - \Phi_{\text{Haar}}^{(k)}\|_{\diamond}^2 \leq d^{2k}(\mathcal{F}_{\mathcal{E}}^{(k)} - \mathcal{F}_{\text{Haar}}^{(k)}), \quad (4)$$

where $d = q^n$ is the Hilbert space dimension, q is the local dimension of the qudits, and $\mathcal{F}_{\text{Haar}}^{(k)} = k!$.

If we obtain the frame potential $\mathcal{F}_{\mathcal{E}}^{(k)}$, we are guaranteed to have at least an ϵ_{\max} -approximate k -design, where

$$\epsilon_{\max} = d^k \sqrt{\mathcal{F}_{\mathcal{E}}^{(k)} - \mathcal{F}_{\text{Haar}}^{(k)}}, \quad (5)$$

Similarly, we have the following condition for the ensemble to be an ϵ -approximate k -design:

$$\sqrt{\mathcal{F}_{\mathcal{E}(l)}^{(k)} - \mathcal{F}_{\text{Haar}}^{(k)}} \leq \frac{\epsilon}{q^{nk}}, \quad (6)$$

where the ensemble $\mathcal{E}(l)$ depends on the number of layers l . Assuming an exponentially decreasing frame potential approaching the Haar value, we have

$$\mathcal{F}_{\mathcal{E}(l)}^{(k)} - \mathcal{F}_{\text{Haar}}^{(k)} \propto A^2 e^{-2l/C} \quad (7)$$

$$\Rightarrow A e^{-l/C} \leq \frac{\epsilon}{q^{nk}} \quad (8)$$

$$\Rightarrow l \geq C(kn \log q + \log A + \log 1/\epsilon). \quad (9)$$

Under this assumption, A and C could still have n and k dependence. Therefore, for there to be linear scaling in n and k , A cannot be exponential, and C must be sublinear.

As an example, the exponential decay of $\mathcal{F}^{(2)}$ for the parallel random unitary ansätze is given by [18]

$$\mathcal{F}^{(2)} < 2 \left(1 + \left(\frac{2q}{q^2 + 1} \right)^{2(l-1)} \right)^{n_g - 1}, \quad (10)$$

where $n_g = \lfloor n/2 \rfloor$. This is plotted in Fig. 1. For fixed ϵ , this leads to a linear scaling of l in n , given by

$$l \geq C(2n \log q + \log n + \log 1/\epsilon), \quad (11)$$

where $C = \left(\log \frac{q^2 + 1}{2q} \right)^{-1}$ is independent of n . We emphasize that linear scaling in n is for fixed ϵ , not fixed \mathcal{F} .

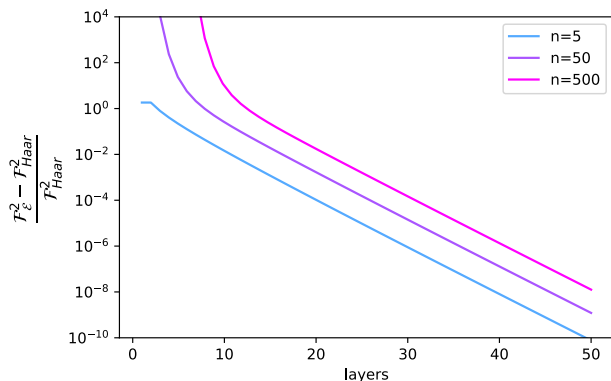


FIG. 1. Theoretical percentage deviation of the $k = 2$ frame potential from the Haar value as a function of layers for the parallel random unitary ansätze. In this plot, the layer required to reach a fixed \mathcal{F} does not scale linearly with n . The linear scaling is only for fixed ϵ .

III. EVALUATION OF FRAME POTENTIAL

The unitary ensembles we are interested in are parameterized by a large number of parameters. Therefore, evaluating the integral is a high-dimensional integration problem, and a numerical Monte Carlo approach is suitable. We approximate the frame potential as the mean value of the trace,

$$\mathcal{F}_{\mathcal{E}}^{(k)} \approx \frac{1}{N} \sum |\text{Tr}(U^\dagger V)|^{2k}, \quad U, V \in \mathcal{E}. \quad (12)$$

Therefore, we need to evaluate the trace of the sampled unitaries on n target qubits.

A. Complexity of Trace Estimation

Explicitly constructing the unitaries requires memory complexity of $O(4^n)$. A more efficient classical algorithm decomposes a unitary into gates in a universal set (H , T , and CNOT), which allows us to estimate the normalized trace by sampling allowed Feynman paths [65]. Exact evaluation using this method is NP complete, and approximation to fixed precision requires a number of Feynman path samples that are exponentially large in the number of Hadamard gates in the circuit.

However, a mixed-state quantum algorithm exists that can estimate the trace efficiently with the DQC1 circuit [66, 67]. Specifically, in order to evaluate the trace of an n -qubit unitary U , only one pure-state special qubit is needed. A Hadamard gate is applied to the special qubit, and the U gate is applied to the n -qubit maximally mixed state, controlled by the special qubit. The complexity is independent of n and polynomial to the precision.

To bridge the gap between the classical and quantum complexity, we propose a classical tensor-network-based algorithm for *exact* shallow circuits trace evaluation. For shallow circuits, a tensor network simulator can obtain, with $O(n)$ complexity, single-probability amplitudes

$$\langle \Psi | {}_i U | \Psi \rangle_j \quad (13)$$

for any computational basis states $|\Psi\rangle_i$ and $|\Psi\rangle_j$. Evaluating the trace of a unitary requires 2^n evaluations for all basis states. This naive implementation of tensor network simulators is already significantly more efficient than the state vector approach for shallow circuits, but it is still intractable. The contribution of our work is to rewrite the trace operation as a single amplitude, reducing to *linear* complexity in n .

B. Algorithm Description

A quantum circuit unitary $U = U_1 U_2 U_3 \dots$ is a tensor $U_{ijk\dots}^{\alpha\beta\gamma\dots}$, where i, j, k are input qubit indices and α, β, γ are output qubit indices. The trace of the unitary is

$$\text{Tr}(U) = \sum_{ijk\dots\alpha\beta\gamma\dots} U_{ijk\dots}^{\alpha\beta\gamma\dots} \delta_{i\alpha} \delta_{j\beta} \delta_{k\gamma} \dots \quad (14)$$

This is a tensor contraction operation that can be expressed as the tensor network in Fig. 2 a. In this representation, each node is an index, and edges that form cliques are unitaries. The circuit shown here is a parallel random unitary circuit with 4 qubits. The i indices correspond to qubit inputs, and the o indices correspond to qubit outputs. The curves going above the circuit network are identities. The input and output indices can actually be merged together, but this is harder to illustrate. For efficient contraction when the number of qubit is large, the contraction order is along the direction indicated on the figure such that the maximum number of exposed indices is minimum throughout contraction.

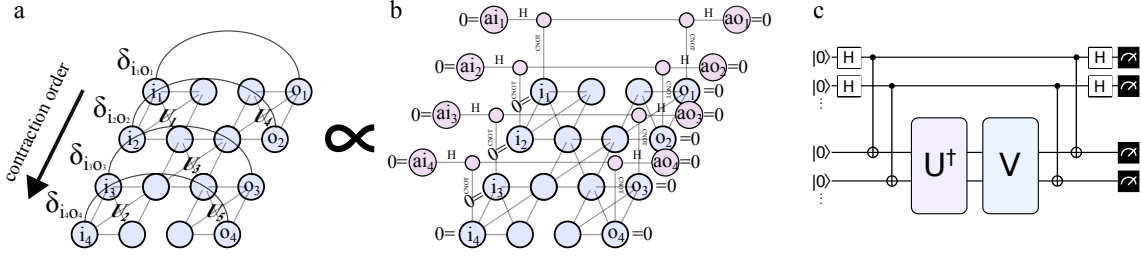


FIG. 2. (a) Graphical tensor network representation of the trace of a quantum circuit. (b) Graphical tensor network representation of the same quantity using our formulation. (c) The quantum circuit used to evaluate traces as a single amplitude.

Directly implementing this tensor network requires modification of QTensor. We propose an alternative tensor network in Fig. 2 b with similar topologies that gives the trace as a single-probability amplitude in the form of E.q. 13. The quantum circuit to achieve this is illustrated in Fig. 2 c, and we proceed with a proof.

For simplicity, we describe the algorithm for $q = 2$ qubits. We assign an ancillary qubit to each target qubit. The quantum state of the n ancillary and n target qubits is initialized to the state

$$|\Psi\rangle_0 = |00 \cdots 0\rangle_a \otimes |00 \cdots 0\rangle_t. \quad (15)$$

After a layer of Hadamard on the ancillary qubits, we get

$$|\Psi\rangle \rightarrow \frac{1}{\sqrt{2^n}} \sum_{\mu}^{2^n} |\mu\rangle_a \otimes |00 \cdots 0\rangle_t, \quad (16)$$

where $|\mu\rangle$ are the n ancillary qubit basis states in the computational basis. Applying a CNOT gate on all target qubits controlled by their respective ancillary qubits yields

$$|\Psi\rangle \rightarrow \bigotimes_j^n U_{a=j, t=j}^{\text{CNOT}} \frac{1}{\sqrt{2^n}} \sum_{\mu}^{2^n} |\mu\rangle_a \otimes |00 \cdots 0\rangle_t \quad (17)$$

$$= \frac{1}{\sqrt{2^n}} \sum_{\mu}^{2^n} \bigotimes_j^n U_{a=j, t=j}^{\text{CNOT}} |\mu\rangle_a \otimes |00 \cdots 0\rangle_t \quad (18)$$

$$= \frac{1}{\sqrt{2^n}} \sum_{\mu}^{2^n} |\mu\rangle_a \otimes |\mu\rangle_t, \quad (19)$$

$$|\Psi\rangle = M|\Psi\rangle_0, \quad (20)$$

where M is related to the measurement basis later. Consider the following probability amplitude:

$$\langle \Psi | U^\dagger V | \Psi \rangle = \langle \Psi |_0 M U^\dagger V M | \Psi \rangle_0. \quad (21)$$

This is simply the probability amplitude of measuring the $|\Psi\rangle_0$ state after applying the unitary $M U^\dagger V M$ to the initialized $|\Psi\rangle_0$ state. Moreover, this probability amplitude

is actually the trace of $U^\dagger V$:

$$\begin{aligned} \langle \Psi | U^\dagger V | \Psi \rangle &= \frac{1}{2^n} \left(\sum_{\mu}^{2^n} \langle \mu |_a \langle \mu |_t \right) U^\dagger V \left(\sum_{\nu}^{2^n} |\nu\rangle_a |\nu\rangle_t \right) \\ &= \frac{1}{2^n} \sum_{\mu}^{2^n} \langle \mu |_t U^\dagger V | \mu \rangle_t = \frac{1}{2^n} \text{Tr} (U^\dagger V). \end{aligned} \quad (22)$$

Therefore, evaluating the trace becomes evaluating the probability amplitude of obtaining the $|\Psi\rangle_0$ state, which QTensor is able to simulate with complexity proportional to the number of qubits and exponential to the circuit depth. This is helpful for evaluating the trace of unitaries that can be efficiently represented by shallow circuits, especially those with limited qubit connectivity such as hardware-efficient ansätze.

For qudits with general local dimensions q , the generalization is straightforward. We need to replace the Hadamard gate H with the generalized Hadamard gate H_q and the CNOT gate with the SUM_q gate [68]:

$$H_q |j\rangle = \frac{1}{\sqrt{q}} \sum_{i=0}^{q-1} e^{2\pi i j / q} |i\rangle \quad (24)$$

$$\text{SUM}_q |i, j\rangle = |i, i + j \pmod{q}\rangle. \quad (25)$$

Similar to the qubit case, applying the generalized gates to $|\Phi\rangle_0$ yields an entangled uniform superposition $|\Phi\rangle$ of all basis states. The expectation value of any target qudit unitary with respect to this state is the trace.

IV. RESULTS

We obtain numerical results for ansätze with local dimension $q = 2$. Specifically, the frame potential values up to 50 qubits and $k = 5$ are evaluated.

A. Verifying the Brown–Susskind Conjecture from Frame Potentials

We compute the frame potentials for local random unitary ansätze and parallel random unitary ansätze. For

parallel random unitaries, each layer is a wall of two-qudit random unitaries on neighboring qudits, and the next layer is offset by 1 qudit. This creates a brickwork motif, and the gate count scales as $O(ln)$. For local random unitaries, each layer is a single two-qudit random unitary between a pair of randomly chosen neighboring qudits. The gate count scales as $O(l)$. For both ansätze, the random unitaries are drawn from the Haar measure on $U(d^2)$. Both are illustrated in Fig. 3

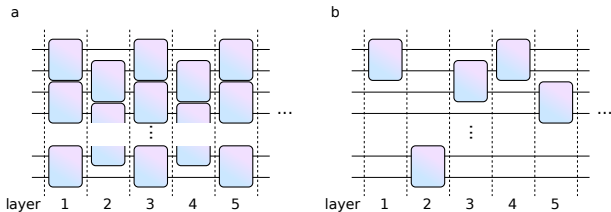


FIG. 3. (a) Parallel random unitary ansätze. (b) Local random unitary ansätze.

1. Parallel Random Unitaries

Results for parallel random unitaries are presented in Figs. 4, 5, and 6. In Fig. 4, The frame potential shows a super-exponential decay in the regime of few layers and converges to exponential decay as the number of layer increases, just like the theoretical prediction in Fig. 1.

To obtain the layer scaling for reaching ϵ -approximate designs, we manipulate Eq. 5, obtaining

$$\log \epsilon_{\max}(l) = nk \log 2 + \frac{1}{2} \log(\mathcal{F}_{\mathcal{E}(l)}^{(k)} - \mathcal{F}_{\text{Haar}}^{(k)}), \quad (26)$$

and fit $\log \epsilon_{\max}$ to $al + b$ within suitable ranges of l . The fitted curves are extrapolated to find the numbers of layers needed to intersect the desired ϵ value. Note that our numerical results are in the regime of large ϵ but we are extrapolating to small ϵ values, the validity of which depends on a tightly exponentially decaying \mathcal{F} .

Assuming the validity of extrapolation, the results for $\epsilon = 0.1$ are shown in Figs. 5 and 6. Because of the large uncertainties for large k and n , we do not show those data points. We observe a linear scaling of the number of needed layers in n , which agrees with the theoretical prediction and nontrivially restricts the \mathcal{F} scale factor A and decay rate C , as discussed in Section II.

Further, we compare the theoretical predictions in Eq. 11 against our numerical findings. Figure 6 shows the experimental and fitted 2-design layer scaling as a function of the number of qubits. Specifically, we fit a linear curve, ignoring the $\log n$ and the constant $\log 1/\epsilon$ terms. We find a slope of 4.89, which is lower than the theoretical value 6.2. We note, however, that the theoretical value gives an upper bound of the frame potential, since there is overcounting in the contributing domain

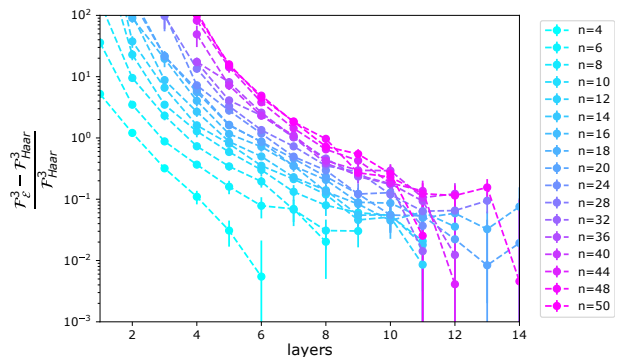


FIG. 4. Percentage deviation of the $k = 3$ frame potential from the Haar value as a function of layers for the parallel random unitary ansätze. As shown in Fig. 1, we do not expect linear scaling of l in n with fixed \mathcal{F} .

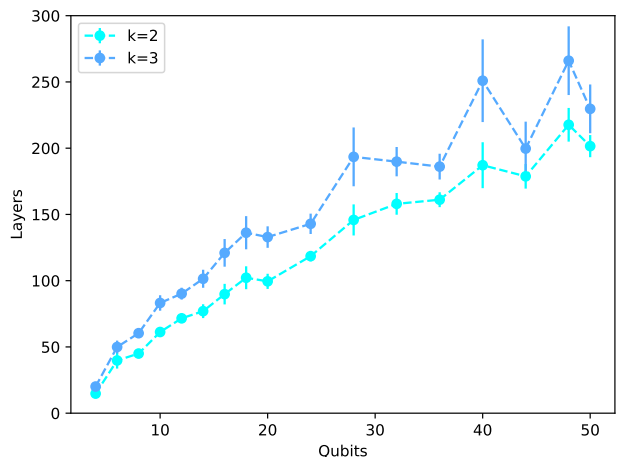


FIG. 5. Layer scaling as a function of the number of qubits for the parallel random unitary ansätze.

walls [18]. Therefore, the analytical expression predicts a larger number of layers needed to approximate 2-designs than necessary. This is apparent in the $n = 2$ case, where 16 layers are needed in Eq. 11 but a single layer is already sampling from the Haar measure. This accounts for the discrepancy between the theoretical values and the experimental values.

In the inset of Fig. 6, we show the slopes of the scaling curves with different k values. It is predicted that there is a linear $O(nk)$ scaling in k for the number of layers l (or $O(n^2k)$ scaling for the circuit size T) needed to approach k -designs [18], and a linear relationship between k and complexity is established in [47]. Together, these findings imply that complexity grows linearly in the circuit size [47, 50]. Our results support the linear scaling of T in k , which predicts that the slope grows linearly in k .

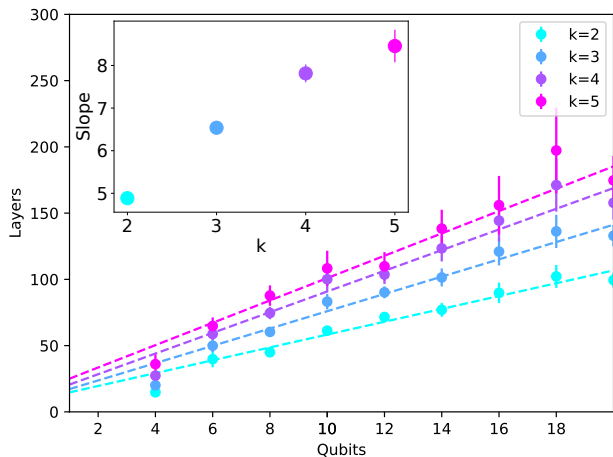


FIG. 6. Experimental and fitted 2-design layer scaling as a function of the number of qubits for the parallel random unitary ansätze. Fitting is performed on data points from $n = 6$ to $n = 18$. The inset shows the fitted slopes for different k values.

2. Local Random Unitaries

Results for local random unitaries are presented in Figs. 7 and 8. Since each layer in the local random circuit has only one gate, we simulate layers proportional to the number of qubits and plot layers/qubits on the x -axis to maintain a linear scaling. We observe that this layer/qubits ratio scales linearly with the number of qubits. This is the same gate count scaling as the parallel random unitary ansätze, both quadratic in n . The scaling in k is too noisy to draw conclusions.

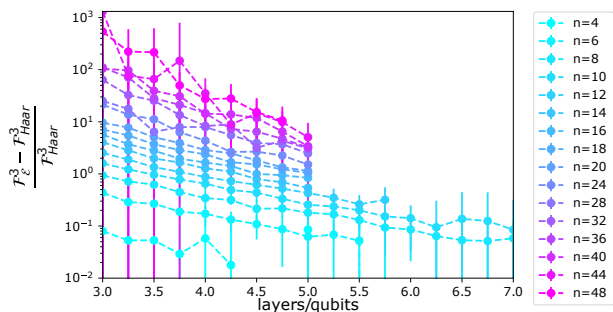


FIG. 7. Percentage deviation of the $k = 3$ frame potential from the Haar value as a function of layers over the number of qubits for the local random unitary ansatz.

B. Hardware-Efficient Ansätze as Approximate k -Designs

Originally proposed as ansätze for variational quantum eigensolvers [53], hardware-efficient ansätze utilize gates

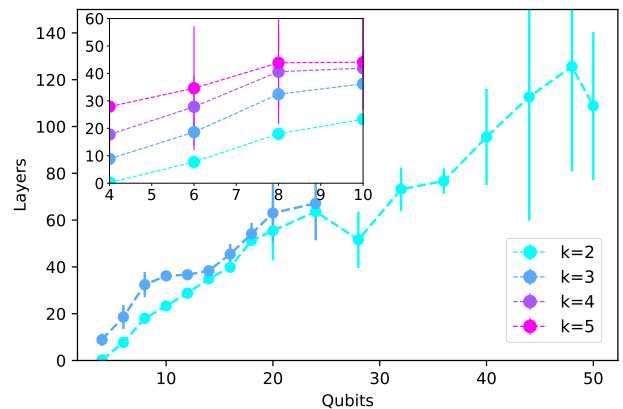


FIG. 8. Layer/qubits scaling as a function of the number of qubits for the local random unitary ansätze. The inset shows larger k values for few qubits. Results for large k 's and n 's are noisy and not plotted.

and connectivity readily available on the quantum hardware and are attractive because of their relaxed hardware requirements. The ansätze are simulated in the context of the barren plateau problem [21], where a wall of $R_Y(\pi/4)$ rotations is followed by alternating layers of random Pauli rotations and controlled-phase gates, as illustrated in Fig. 9. Figure 10 shows that \mathcal{F} decreases exponentially. Figure 11 shows a linear dependence on the number of qubits as well as k .

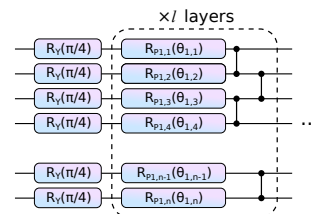


FIG. 9. (a) Parallel random unitary ansätze. (b) Local random unitary ansätze.

We note that these ansätze reach lower frame potential values with much fewer layers, albeit having much fewer parameters per layer. This result is partially explainable through the observation that each layer in the hardware-efficient ansätze contains two layers of two-qubit gate walls, whereas each layer in the parallel random unitary ansätze contains only one wall. Further, random unitaries from $U(d^2)$ are not all maximally entangling. The hardware-efficient ansätze can therefore generate highly entangled stages much more efficiently, exploring a much larger space with fewer parameters.

Further, unlike the previously discussed ansätze where the frame potential decay rate is constant, the hardware-efficient ansätze decay rate increases with n as shown in the inset of Fig. 10. This does not contradict the observed linear scaling as long as the decay rate scaling

is sublinear.

This observation confirms that hardware-efficient ansätze are highly expressive, a concept that is crucial to the utility of variational quantum algorithms. Ansätze with higher expressibility are able to better represent the Haar distribution and therefore able to better approximate the target unitary or minimize the objective. This links the expressibility to the frame potential [69]. The high expressibility of hardware-efficient ansätze and their close relatives, and consequently the desirable noise properties due to their shallow depths, are precisely the argument in favor of these ansätze over their deeper and more complex problem-aware counterparts [70]. With the recent discovery of the relation between expressibility and gradient variance [71], the analysis of frame potentials can play an important role in theoretically and empirically determining the usefulness of various ansätze for variational algorithms.

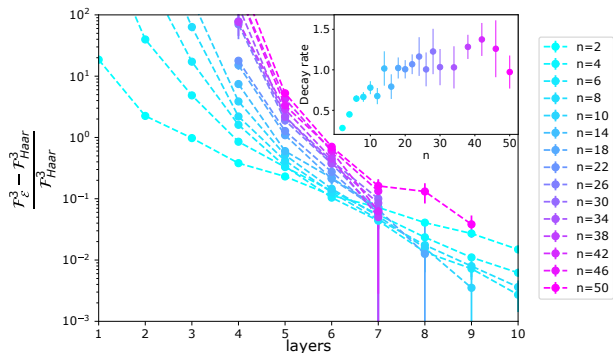


FIG. 10. Percentage deviation of the $k = 3$ frame potential from the Haar value as a function of layers for the hardware-efficient ansätze. The inset shows the decay rate scaling of \mathcal{F} in the number of qubits n .

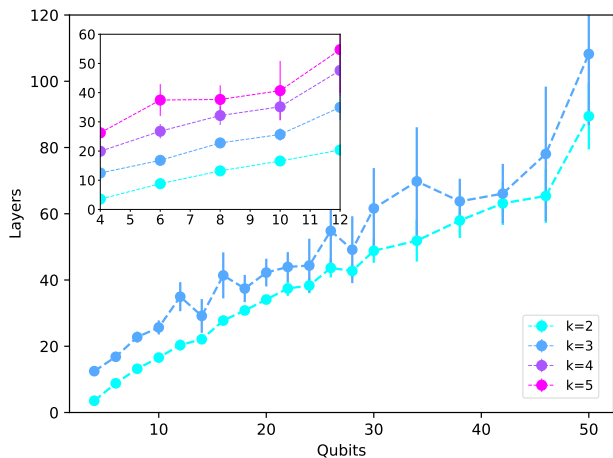


FIG. 11. Layer scaling as a function of the number of qubits for the hardware-efficient ansätze.

V. CONCLUSION

Evaluating the distance from a given random circuit ensemble to the exact Haar randomness is important for understanding several perspectives in quantum information science, including recent experiments on the near-term quantum advantage. In our paper we present novel classical tensor network simulation algorithms for evaluating the frame potential, the 2-norm distance from a given ensemble to the exact Haar randomness. We describe large-scale random circuit sampling experiments classically up to 50 qubits, the number of noisy physical qubits we are able to control in the NISQ era, using the QTENSOR platform. As examples, we provide two applications of our computational tools: a numerical verification of the Brown–Susskind conjecture and a numerical estimation relating the barren plateau in quantum machine learning and the randomized hardware-efficient variational ansatz.

Through our examples we show that classical tensor network simulations are useful for our understanding of open problems in theoretical computer science and numerical examinations of quantum neural network properties for quantum computing applications. We believe that tensor networks and other cutting-edge tools are useful for probing the boundary of classical simulation and improving the understanding of quantum advantage in several subjects of quantum physics, for instance, quantum simulation [72, 73]. Moreover, it will be interesting to connect our algorithms to the current research on classical simulation of boson sampling experiments.

ACKNOWLEDGMENT

This material is based upon work supported by the U.S. Department of Energy, Office of Science, National Quantum Information Science Research Centers. This work was completed in part with resources provided by the University of Chicago Research Computing Center. We thank Jens Eisert and Danylo Lykov for useful discussions.

Y.A. acknowledges support from the U.S. Department of Energy, Office of Science, under contract DE-AC02-06CH11357 at Argonne National Laboratory and Defense Advanced Research Projects Agency (DARPA) under Contract No. HR001120C0068.

J.L. is supported in part by International Business Machines (IBM) Quantum through the Chicago Quantum Exchange and by the Pritzker School of Molecular Engineering at the University of Chicago through AFOSR MURI (FA9550-21-1-0209). J.L. is also serving as a scientific advisor in qBraid Co.

L.J. acknowledges support from ARO (W911NF-18-1-0020, W911NF-18-1-0212), ARO MURI (W911NF-16-1-0349, W911NF-21-1-0325), AFOSR MURI (FA9550-19-1-0399, FA9550-21-1-0209), AFRL (FA8649-21-P-0781), DoE Q-NEXT, NSF (OMA-1936118, EEC-1941583,

OMA-2137642), NTT Research, and the Packard Foundation (2020-71479).

CODE AND DATA AVAILABILITY

The code used to generate the data and figures is available in the GitHub repository [74]. Data containing the

frame potential values used to generate the figures are available in the same GitHub repository, and data for the calculated trace values of sampled random circuits is available upon request from the authors. The tensor network quantum simulator QTensor and QTensorAI are open source and available [75, 76].

-
- [1] R. P. Feynman *et al.*, *Int. j. Theor. Phys* **21** (1982).
- [2] J. Preskill, arXiv preprint arXiv:1203.5813 (2012).
- [3] Y. Alexeev, D. Bacon, K. R. Brown, R. Calderbank, L. D. Carr, F. T. Chong, B. DeMarco, D. Englund, E. Farhi, B. Fefferman, *et al.*, *PRX Quantum* **2**, 017001 (2021).
- [4] J. Preskill, *Quantum* **2**, 79 (2018).
- [5] F. Arute, K. Arya, R. Babbush, D. Bacon, J. C. Bardin, R. Barends, R. Biswas, S. Boixo, F. G. Brandao, D. A. Buell, *et al.*, *Nature* **574**, 505 (2019).
- [6] H.-S. Zhong, H. Wang, Y.-H. Deng, M.-C. Chen, L.-C. Peng, Y.-H. Luo, J. Qin, D. Wu, X. Ding, Y. Hu, *et al.*, *Science* **370**, 1460 (2020).
- [7] S. Ebadi, A. Keesling, M. Cain, T. T. Wang, H. Levine, D. Bluvstein, G. Semeghini, A. Omran, J. Liu, R. Samajdar, X.-Z. Luo, B. Nash, X. Gao, B. Barak, E. Farhi, S. Sachdev, N. Gemelke, L. Zhou, S. Choi, H. Pichler, S. Wang, M. Greiner, V. Vuletic, and M. D. Lukin, (2022), 10.48550/ARXIV.2202.09372.
- [8] S. R. White, *Physical Review Letters* **69**, 2863 (1992).
- [9] S. Rommer and S. Ostlund, *Physical Review B* **55**, 2164 (1997).
- [10] R. Orus, *Nature Reviews Physics* **1**, 538 (2019).
- [11] K. Noh, L. Jiang, and B. Fefferman, *Quantum* **4**, 318 (2020).
- [12] C. Huang, F. Zhang, M. Newman, J. Cai, X. Gao, Z. Tian, J. Wu, H. Xu, H. Yu, B. Yuan, *et al.*, arXiv preprint arXiv:2005.06787 (2020).
- [13] F. Pan and P. Zhang, arXiv preprint arXiv:2103.03074 (2021).
- [14] C. Oh, K. Noh, B. Fefferman, and L. Jiang, *Physical Review A* **104**, 022407 (2021).
- [15] S. Boixo, S. V. Isakov, V. N. Smelyanskiy, R. Babbush, N. Ding, Z. Jiang, M. J. Bremner, J. M. Martinis, and H. Neven, *Nature Physics* **14**, 595 (2018).
- [16] A. W. Harrow and R. A. Low, *Communications in Mathematical Physics* **291**, 257 (2009).
- [17] F. G. Brandao, A. W. Harrow, and M. Horodecki, *Communications in Mathematical Physics* **346**, 397 (2016).
- [18] N. Hunter-Jones, arXiv preprint arXiv:1905.12053 (2019).
- [19] P. Hayden and J. Preskill, *JHEP* **09**, 120 (2007), arXiv:0708.4025 [hep-th].
- [20] A. Nahum, S. Vijay, and J. Haah, *Phys. Rev. X* **8**, 021014 (2018), arXiv:1705.08975 [cond-mat.str-el].
- [21] J. R. McClean, S. Boixo, V. N. Smelyanskiy, R. Babbush, and H. Neven, *Nature communications* **9**, 1 (2018).
- [22] J. Liu, F. Tacchino, J. R. Glick, L. Jiang, and A. Mezzacapo, (2021), arXiv:2111.04225 [quant-ph].
- [23] J. Liu, K. Najafi, K. Sharma, F. Tacchino, L. Jiang, and A. Mezzacapo, (2022), arXiv:2203.16711 [quant-ph].
- [24] W. Brown and O. Fawzi, *Communications in mathematical physics* **340**, 867 (2015).
- [25] J. Liu, *Phys. Rev. Res.* **2**, 043164 (2020), arXiv:2003.11425 [quant-ph].
- [26] D. A. Roberts and B. Yoshida, *JHEP* **04**, 121 (2017), arXiv:1610.04903 [quant-ph].
- [27] J. Cotler, N. Hunter-Jones, J. Liu, and B. Yoshida, *JHEP* **11**, 048 (2017), arXiv:1706.05400 [hep-th].
- [28] J. Liu, *Phys. Rev. D* **98**, 086026 (2018), arXiv:1806.05316 [hep-th].
- [29] F. G. Brandao and M. Horodecki, arXiv preprint arXiv:1010.3654 (2010).
- [30] D. Harlow and P. Hayden, *Journal of High Energy Physics* **2013**, 1 (2013).
- [31] F. G. Brandao, A. W. Harrow, and M. Horodecki, *Physical Review Letters* **116**, 170502 (2016).
- [32] Z. Ji, Y.-K. Liu, and F. Song, arXiv preprint arXiv:1711.00385 (2017).
- [33] P. Ananth, L. Qian, and H. Yuen, arXiv preprint arXiv:2112.10020 (2021).
- [34] B. Škorić, *International Journal of Quantum Information* **10**, 1250001 (2012).
- [35] G. Gianfelici, H. Kampermann, and D. Bruß, *Physical Review A* **101**, 042337 (2020).
- [36] N. Kumar, R. Mezher, and E. Kashefi, arXiv preprint arXiv:2101.05692 (2021).
- [37] M. Doosti, N. Kumar, E. Kashefi, and K. Chakraborty, arXiv preprint arXiv:2110.11724 (2021).
- [38] M. Arapinis, M. Delavar, M. Doosti, and E. Kashefi, *Quantum* **5**, 475 (2021).
- [39] D. Lykov, A. Chen, H. Chen, K. Keipert, Z. Zhang, T. Gibbs, and Y. Alexeev, in *2021 IEEE/ACM Second International Workshop on Quantum Computing Software (QCS)* (IEEE, 2021) pp. 27–34.
- [40] D. Lykov and Y. Alexeev, arXiv preprint arXiv:2106.15740 (2021), 10.48550/arXiv.2106.15740.
- [41] D. Lykov, R. Schutski, A. Galda, V. Vinokur, and Y. Alexeev, arXiv preprint arXiv:2012.02430 (2020).
- [42] I. T. Diniz and D. Jonathan, *Communications in Mathematical Physics* **304**, 281 (2011).
- [43] A. Harrow and S. Mehraban, arXiv preprint arXiv:1809.06957 (2018).
- [44] Y. Nakata, C. Hirche, M. Koashi, and A. Winter, arXiv preprint arXiv:1609.07021 (2016).
- [45] E. Onorati, O. Buerschaper, M. Kliesch, W. Brown, A. H. Werner, and J. Eisert, *Communications in Mathematical Physics* **355**, 905 (2017).
- [46] N. Lashkari, D. Stanford, M. Hastings, T. Osborne, and P. Hayden, *JHEP* **04**, 022 (2013), arXiv:1111.6580 [hep-th].

- [47] F. G. S. L. Brandão, W. Chemissany, N. Hunter-Jones, R. Kueng, and J. Preskill, *PRX Quantum* **2**, 030316 (2021), arXiv:1912.04297 [hep-th].
- [48] A. R. Brown and L. Susskind, *Phys. Rev. D* **97**, 086015 (2018), arXiv:1701.01107 [hep-th].
- [49] L. Susskind, (2018), arXiv:1802.02175 [hep-th].
- [50] J. Haferkamp, P. Faist, N. B. Kothakonda, J. Eisert, and N. Yunger Halpern, *Nature Physics* , 1 (2022).
- [51] A. Peruzzo, J. McClean, P. Shadbolt, M.-H. Yung, X.-Q. Zhou, P. J. Love, A. Aspuru-Guzik, and J. L. O’Brien, *Nature Communications* **5**, 1 (2014).
- [52] J. R. McClean, J. Romero, R. Babbush, and A. Aspuru-Guzik, *New Journal of Physics* **18**, 023023 (2016).
- [53] A. Kandala, A. Mezzacapo, K. Temme, M. Takita, M. Brink, J. M. Chow, and J. M. Gambetta, *Nature* **549**, 242 (2017).
- [54] M. Cerezo, A. Arrasmith, R. Babbush, S. C. Benjamin, S. Endo, K. Fujii, J. R. McClean, K. Mitarai, X. Yuan, L. Cincio, *et al.*, *Nature Reviews Physics* , 1 (2021).
- [55] E. Farhi, J. Goldstone, and S. Gutmann, arXiv preprint arXiv:1411.4028 (2014).
- [56] P. Wittek, *Quantum machine learning: what quantum computing means to data mining* (Academic Press, 2014).
- [57] N. Wiebe, A. Kapoor, and K. M. Svore, arXiv preprint arXiv:1412.3489 (2014).
- [58] J. Biamonte, P. Wittek, N. Pancotti, P. Rebentrost, N. Wiebe, and S. Lloyd, *Nature* **549**, 195 (2017).
- [59] M. Schuld and N. Killoran, *Physical Review Letters* **122**, 040504 (2019).
- [60] V. Havlíček, A. D. Córcoles, K. Temme, A. W. Harrow, A. Kandala, J. M. Chow, and J. M. Gambetta, *Nature* **567**, 209 (2019).
- [61] Y. Liu, S. Arunachalam, and K. Temme, *Nature Physics* , 1 (2021).
- [62] J. Liu, *Does [Richard Feynman] Dream of Electric Sheep? Topics on Quantum Field Theory, Quantum Computing, and Computer Science*, Ph.D. thesis, Caltech (2021).
- [63] E. Farhi and H. Neven, arXiv preprint arXiv:1802.06002 (2018).
- [64] D. Gross, K. Audenaert, and J. Eisert, *Journal of Mathematical Physics* **48**, 052104 (2007).
- [65] A. Datta, S. T. Flammia, and C. M. Caves, *Physical Review A* **72**, 042316 (2005).
- [66] E. Knill and R. Laflamme, *Phys. Rev. Lett.* **81**, 5672 (1998).
- [67] R. Laflamme, E. Knill, D. Cory, E. Fortunato, T. Havel, C. Miquel, R. Martinez, C. Negrevergne, G. Ortiz, M. Pravia, *et al.*, arXiv preprint quant-ph/0207172 (2002).
- [68] Y. Wang, Z. Hu, B. C. Sanders, and S. Kais, *Front. Phys.* **8** (2020), 10.3389/fphy.2020.589504.
- [69] S. Sim, P. D. Johnson, and A. Aspuru-Guzik, *Advanced Quantum Technologies* **2**, 1900070 (2019).
- [70] X. Liu, A. Angone, R. Shaydulin, I. Safro, Y. Alexeev, and L. Cincio, *IEEE Transactions on Quantum Engineering* **3**, 1 (2022).
- [71] Z. Holmes, K. Sharma, M. Cerezo, and P. J. Coles, *PRX Quantum* **3**, 010313 (2022).
- [72] X. Yuan, J. Sun, J. Liu, Q. Zhao, and Y. Zhou, *Phys. Rev. Lett.* **127**, 040501 (2021), arXiv:2007.00958 [quant-ph].
- [73] A. Milsted, J. Liu, J. Preskill, and G. Vidal, *PRX Quantum* **3**, 020316 (2022), arXiv:2012.07243 [quant-ph].
- [74] M. Liu, “Frame_potential,” https://github.com/sss441803/Frame_Potential (2022).
- [75] M. Liu, <https://github.com/sss441803/QTensorAI> (2022).
- [76] D. Lykov, <https://github.com/danlkv/QTensor> (2020).

Supplementary Material: Estimating the frame potential of large-scale quantum circuit sampling using tensor networks up to 50 qubits

Minzhao Liu,^{1,2,*} Junyu Liu^{*,3,4,5,6,†} Yuri Alexeev,^{2,4,‡} and Liang Jiang^{3,4,§}

¹*Department of Physics, The University of Chicago, Chicago, IL 60637, USA*

²*Computational Science Division, Argonne National Laboratory, Lemont, IL 60439, USA*

³*Pritzker School of Molecular Engineering, The University of Chicago, Chicago, IL 60637, USA*

⁴*Chicago Quantum Exchange, Chicago, IL 60637, USA*

⁵*Kadanoff Center for Theoretical Physics, The University of Chicago, Chicago, IL 60637, USA*

⁶*qBraid Co., Harper Court 5235, Chicago, IL 60615, USA*

*: Corresponding author.

CONTENTS

I. Introduction to QTensor	1
II. Simulation details	1
A. Sampling $U(d^2)$	1
B. High-Performance Computing	2
C. Other Details	2
References	2

I. INTRODUCTION TO QTENSOR

For all the trace evaluations, we use the QTensorAI library [1], originally developed to simulate quantum machine learning with parameterized circuits. This library allows quantum circuits to be simulated in parallel on CPUs and GPUs, which is a highly desirable property for sampling a large number of circuits. The library is based on the QTensor simulator [2–4], a tensor network-based quantum simulator that represents the network as an undirected graph.

In this method of simulation, the computation is memory bound, and the memory complexity is exponential in the “tree width,” the largest rank of tensor that needs to be stored during computation. The graphical formalism utilized by QTensor allows the tensor contraction order to be optimized to minimize the tree width. For shallow quantum circuits, the tree width is determined mainly by the number of layers in the quantum circuit, and therefore QTensor is particularly well suited for simulating shallow circuits such as those used in the Quantum Approximate Optimization Algorithm (QAOA).

II. SIMULATION DETAILS

A. Sampling $U(d^2)$

The simulation of both parallel and local random unitary circuits require the use of random two-qubit random unitary gates. We implement these gates and sample Haar unitaries according to the scheme proposed for unitary neural networks [5], using a PyTorch implementation [6]. This implementation parameterizes two-qubit unitaries using 16 phase parameters, and uniformly sampling these parameters leads to uniform sampling on the Haar measure. Further, it is fully differentiable, although we do not care about this property in this work.

* mliu6@uchicago.edu

† junyuliu@uchicago.edu

‡ yuri@alcf.anl.gov

§ liangjiang@uchicago.edu

B. High-Performance Computing

For hardware-efficient and parallel random unitary ansätze, once the number of qubits and the number of layers are chosen, the circuit topology will remain the same throughout the ensemble. This is in contrast to the local random unitary ansätze, where a two-qubit gate is applied to random neighboring qubits in each layer, which means that the circuit topologies are very different within an ensemble. For fixed-topology ensembles, the algorithm can optimize the contraction order for all circuits at once. This optimization significantly reduces the computational complexity, and the optimization time is on the order of minutes depending on the circuit size. However, local random unitary circuits cannot benefit from circuit optimizations since we would need to do that for each sample, whereas the actual simulation time is usually much shorter.

Further, for fixed topology circuits, the tensor contraction operations are identical, which is very suitable for single-instruction multi-data parallel executions on GPUs. For ensembles with the smallest tree widths, we can compute the trace values of millions of circuits in parallel on a single GPU. However, local random unitary circuits are not compatible with single-instruction parallel computation, and must be simulated in parallel using a CPU cluster.

C. Other Details

We compute and store the individual trace values for each sampled circuit, and use the same trace values to compute frame potentials with different k values. Therefore, there is a correlation between the computed frame potentials for different k 's. For example, the layer scaling for the parallel random unitary ansätze shows some correlated fluctuations for both $k = 2$ and $k = 3$. However, if we split the data into three equal partitions and three plot $k = 2$ traces, such fluctuations are no longer correlated, therefore do not represent genuine patterns.

Since the simulation of large circuits is expensive, we adaptively terminate simulations based on the calculated uncertainties in the frame potential. These uncertainties are used later to inform linear curve fitting of $\log_{10}(\epsilon_{\max})$ as a function of n , and the determination of the layers l needed for ϵ_{\max} to intersect with the target ϵ value for the ensemble to be an ϵ -approximate k -design.

-
- [1] H. Liu, J. Liu, R. Liu, H. Makhanov, D. Lykov, A. Apte, and Y. Alexeev, arXiv preprint arXiv:2204.04550 (2022).
 - [2] D. Lykov, A. Chen, H. Chen, K. Keipert, Z. Zhang, T. Gibbs, and Y. Alexeev, in *2021 IEEE/ACM Second International Workshop on Quantum Computing Software (QCS)* (IEEE, 2021) pp. 27–34.
 - [3] D. Lykov and Y. Alexeev, arXiv preprint arXiv:2106.15740 (2021), 10.48550/arXiv.2106.15740.
 - [4] D. Lykov, R. Schutski, A. Galda, V. Vinokur, and Y. Alexeev, arXiv preprint arXiv:2012.02430 (2020).
 - [5] L. Jing, Y. Shen, T. Dubcek, J. Peurifoy, S. Skirlo, Y. LeCun, M. Tegmark, and M. Soljačić, in *International Conference on Machine Learning* (PMLR, 2017) pp. 1733–1741.
 - [6] F. Laporte, “torch_eunn,” https://github.com/flaport/torch_eunn (2020).